Journal of Solid Mechanics Vol. 8, No. 2 (2016) pp. 384-402

Crack Tip Constraint for Anisotropic Sheet Metal Plate Subjected to Mode-I Fracture

R. Kacker , S. S. Bhadauria*

Department of Industrial and Production Engineering, National Institute of Technology, Jalandhar, India

Received 14 March 2016; accepted 12 May 2016

ABSTRACT

On the ground of manufacturing, sheet metal parts play a key role as they cover about half of the production processes. Sheet metals are commonly obtained from rolling and forming processes which causes misalignment of micro structure resulting obvious anisotropic characteristics and micro cracks. Presence of micro cracks poses serious attention, when stresses at the tip reach to the critical value. Present research deals with a thin anisotropic plate, containing an edge crack subjected to mode-I condition. To predict the nature of crack propagation, anisotropic triaxiality is formulated with special reference to Lankford's coefficient and degree of anisotropy. The distribution of magnitude of anisotropic triaxiality is shown with respect to polar angle at crack tip supplemented by plastic zone shapes. Numerical evaluation has been carried out by considering five different cases of plane stress condition using Hill-von Mises yield criteria. Critical values so obtained apropos respective cases, as traced on the yield locus had been used to predict the location of crack propagation in sheet metal. It is revealed that the angle through which the crack propagate do not remain invariable for all combinations of Lankford's coefficient and degree of anisotropy but it shifts for two of the five cases taken into consideration.

Keywords : Triaxiality; Lankford's coefficient; Mode I Fracture; Degree of anisotropy; Hill von mises criteria.

1 INTRODUCTION

SHEET metal parts have substantial significance in the field of manufacturing, as it accounts for nearly half of the overall production. Before any deformation in a random structure, the mechanical properties of the material remain equal in all directions and material posses' isotropic nature. Straining the material, for example subjecting metal to rolling process, the slip planes of material rotate and produce noticeable alignment (preferred orientation) of crystals commonly known as texture, leading the material to develop certain directionality or anisotropic nature, with emergence of tiny micro-cracks. The tip of such micro-crack becomes critical and start propagating along the direction, where stress components reach their maximum value and plastic zone envelop shrinks to minimum. This article considers the problem of such rolled sheet metal plate containing edge crack under plane stress condition subjected to mode-I loading. The crack tip constraint, denoted henceforth in this article as 'Z' and signifying stress triaxiality for anisotropic material, has been investigated.

The idea of investigating such a ratio originates from well-known ductile fracture parameter stress triaxiality. Stress triaxiality is well defined as ratio of hydrostatic stress to von Mises equivalent stresses. This stress

*Corresponding author.
E-mail address: bhadauriass@nitj.ac.in (S.S. Bhadauria).

triaxiality differ mathematically from Z in the sense that the term triaxiality in its denominator contain von Mises equivalent stresses, instead Z contain Hill's equivalent stresses correspondingly. Since the problem dealt is specifically related to anisotropic phenomenon, therefore, it become important to involve the effects of anisotropic parameters such as Lankford coefficient and degree of anisotropy. Thus, to fulfill this requirement instead of stress triaxiality, Z is formulated. The involvement of such parameters is useful because they relate to material behavior. R is a significant formability, apart from being an anisotropy parameter. R-value plays a crucial role in being a formability parameter and along with, it is also a significant anisotropy parameter in software for simulating plastic forming processes therefore defining its accurate value is significant.

Crack propagation leading to fracture has been studied through various parameters at crack tip viz. stress, strain, strain energy density etc. In addition to these factors researchers have also depicted the utility of stress triaxiality as illustrated in literature. Stress triaxiality has been used to signify the effects of microstructures, the lode parameter, temperature and strain rate on ductility of metals [1]. Mechanical behavior was considered through a model on mineral filled PVC and HDPE tensile bars under a variety of triaxialities. Yield stress and plastic dilation were considered as input parameters to evaluate the yield function and flow potential of the developed model. Though yield stress of HDPE barely altered but plastic dilation got bigger with increasing stress triaxiality [2]. On forecasting the value of stress triaxiality ductile fracture was estimated [3]. Within the structure of material martensitic volume and stress triaxiality bands were found to be interdependent and with increase in former, later also increased [4]. Modified Gurson model was developed using stress triaxiality ratio when tests were performed on Al 2024-T351 for simulating damage growth and ductile behavior [5].The effect of stress triaxiality along with strain rate and temperature were studied on the fracture properties of Ti6Al4V [6]. The combined effect of stress triaxialities, crystallographic orientations and growth and coalescence of void were studied in FCC single crystals [7]. Stress triaxiality affected fracture behavior significantly[8]. In the study of ductile materials different damage modes were found to be dependent on stress triaxiality along with Lode parameter [9]. Critical void volume fraction in terms of stress triaxiality was shown in coalescence model of micro-voids in case of ductile materials [10]. With varying stress triaxiality, fracture modes and texture of fracture surfaces were found to be changeable [11]. Beside stress triaxiality equivalent strain was found to be another most significant aspect leading crack formation. Other causes such as stress and strain ratio were inferior [12]. Such value of stress triaxiality was methodically determined beneath which fracture could not be happen [13]. Beside strain intensity, stress triaxiality has been the parameter that control initiation of ductile fracture [14]. Crack tip stress triaxiality was countable on several input parameters like degree of strength mismatch, slenderness of the weld and the crack location within the weld when strength of uneven welded joints were studied near vicinity of crack[15]. Ductility of the material in smoothed and notched specimens were found to be reliant significantly on stress triaxiality [16]. Stress triaxiality had been used as a display for fracture of a building in the Los Angeles area, which suffered excessive damage during Northridge earthquake[17]. Stress triaxiality that builds up subsequent to very slow rate deformation includes a fairly slight effect on cavity growth rate parameter [18]. Strength regarding adhesives layers of dissimilar joints was investigated and it revealed that yield and failure stresses were dependent on the stress triaxiality [19].

The outcome of literature review suggests that the researchers have found stress triaxiality to be a key parameter in ductile fracture. Stress triaxiality is found to be linked with multiple criteria like yielding, failure, cavity growth, plastic strain, coalescence of micro voids, ductility, fracture toughness etc. but regarding anisotropy problem very few researchers have analyzed the combined effects of Lankford's coefficient and degree of anisotropy in mathematical framework of M- criteria containing Hill's equivalent stresses. In this paper, the author attempts to investigate the effect of critical value of crack tip constraint for anisotropic plate. Yield locus has also been plotted for different degrees of anisotropy & Lankford's coefficient in order to identify expected location of crack propagation on it.

2 METHODOLOY

Hill's Eqs. (7-11) of equivalent stress for anisotropic plane stress condition are available for five different cases [22]. These equations are obtained from Hill's generalized equation of anisotropy. This generalized equation contains six constants namely F, G, H, A, B, C .These constants are related to normal and shear yield stresses of material in three perpendicular directions respectively. Equating these constants to zero, mathematically show that yield stress of material in a particular direction can be expressed in terms of yield stress in other directions; signifying the existence of a definite relationship among these yield stresses in three perpendicular directions.

These equations mathematically can be looked as comprising of two parts. The right hand side of the equation signifies material's yield stress and left hand side depicting a combination of anisotropic parameters *R* and *m* along with principal stresses. On taking, left hand side of the equation i.e. Hill's equivalent stresses as denominator, and hydrostatic stresses as numerator, a ratio have been formulated at crack tip for five different cases. Numerical evaluation of Z has been done and plotted with respect to polar angle θ at crack tip. Development of plastic zone at crack tip and plotting its shape has also been done to support the study.

Classical LEFM (Linear Elastic fracture mechanics) theory has been used in present study. In case for further large deformations the concepts can be extended to EPFM (Elasto-Plastic Fracture Mechanics).

3 MATHEMATICAL FORMULATION

3.1 Crack tip constraint, Z

Stress triaxiality, forms the basis for formulation of *Z*, as a crack tip constraint. Though it is defined as the ratio of hydrostatic stress to von Mises equivalent stresses, it can also be looked as the ratio of two parts of a stress tensor, numerator part (hydrostatic stresses) responsible for volumetric changes and denominator (equivalent stresses) for yielding. Formulation of *Z* is the modified form of stress triaxiality that can be used for anisotropic materials. The formulation has been done for *M* and then subsequently *Z*, and further while plotting the curves it is also shown that for a particular value of anisotropic parameters *R* and *m* i.e. *R*=1 and *m*=2, the *Z*-curve and *M* curve are same. *M* (Stress triaxiality) can be expressed as:

$$M = \frac{\sigma_h}{\sigma_{eqv}} \tag{1}$$

Hydrostatic stress under plane stress condition ($\sigma_3 = 0$) is given by $\sigma_h = \frac{\sigma_1 + \sigma_2}{3}$ von Mises equivalent stress under plane stress condition can be expressed as:

$$\sigma_{eqv} \approx \sigma_y = \sqrt{\sigma_1^2 + \sigma_2^2 - \sigma_1\sigma_2} \tag{2}$$

Mathematically stress tensor shows that this combination of stresses can be equated to yield stress. In Cartesian coordinate system principal stresses σ_1 and σ_2 for Mode-I type of fracture at crack tip can be expressed as:

$$\sigma_{1,2} = \frac{K_I}{\sqrt{2\pi r}} \cos\frac{\theta}{2}\left(1 \pm \sin\frac{\theta}{2}\right) \tag{3}$$

At the onset of small scale yielding, classical LEFM theory at crack tip is taken into consideration. On substituting Eq. (3) in Eq. (1) the expression of *M* (stress triaxiality) for mode-I fracture under plane stress condition is obtained as (for full derivation see Appendix (a))

$$M = \frac{2\cos\frac{\theta}{2}}{\sqrt{3\left(\cos^2\frac{\theta}{2}\left(1 + 3\sin^2\frac{\theta}{2}\right)\right)}} \tag{4}$$

Hill [27] proposed generalized yield criteria which has the form

$$\begin{aligned} &F\,|\sigma_2 - \sigma_3|^m + G\,|\sigma_3 - \sigma_1|^m + H\,|\sigma_1 - \sigma_2|^m + A\,|2\sigma_1 - \sigma_2 - \sigma_3|^m \\ &+ B\,|2\sigma_2 - \sigma_3 - \sigma_1|^m + C\,|2\sigma_3 - \sigma_1 - \sigma_2|^m - \sigma_Y^m \le 0 \end{aligned} \tag{5}$$

The general expression of *R*-value [28] or Lankford coefficient can be expressed as:

$$R = \frac{(2^{m-1}+2)\mathrm{A} - C + H}{(2^{m-1}-1)A + 2C + F} \tag{6}$$

where *F, G* and *H* are constants related to normal yield stress of the material in all three orthogonal directions whereas *A*, *B* and *C* are constants that are related to shear yield stresses of the material. Under plane stress condition with some assumptions (i.e. relations amongst the normal and shear yield stresses, for details see Appendix (b)) of detail the generalized Hill's criteria can take different forms [22]

Case I: A=B=0,F=G,H=0

$$\left(\frac{1+2R}{1+R}(|\sigma_1|^m + |\sigma_2|^m) - \frac{R}{1+R}|\sigma_1+\sigma_2|^m\right)^{\frac{1}{m}} \le \sigma_Y \tag{7}$$

Case II: A=B,C=0,F=G=0

$$\left(\begin{array}{l}\dfrac{2^{m-1}(1-R)+(R+2)}{\left(1-2^{m-1}\right)(1+R)}(|\sigma_1-\sigma_2|^m) \\ -\dfrac{1}{\left(1-2^{m-1}\right)(1+R)}(|2\sigma_1-\sigma_2|^m + |2\sigma_2-\sigma_1|^m)\end{array}\right)^{\frac{1}{m}} \le \sigma_Y \tag{8}$$

Case III: A=B,C=0,F=G,H=0

$$\left(\begin{array}{l}\dfrac{2^{m-1}(1-R)+(R+2)}{\left(2+2^{m-1}\right)(1+R)}(|\sigma_1|^m + |\sigma_2|^m) \\ +\dfrac{R}{\left(2+2^{m-1}\right)(1+R)}(|2\sigma_1-\sigma_2|^m + |2\sigma_2-\sigma_1|^m)\end{array}\right)^{\frac{1}{m}} \le \sigma_Y \tag{9}$$

Case IV: A=B=0,F=G=0

$$\left(\frac{1+2R}{2(1+R)}|\sigma_1-\sigma_2|^m + \frac{1}{2(1+R)}|\sigma_1+\sigma_2|^m\right) \le \sigma_Y \tag{10}$$

Case V:A=B=C=0,F=G, (also known as Hosford's yield criteria)

$$\left(\frac{1}{(1+R)}(|\sigma_1|^m + |\sigma_2|^m) + \frac{R}{(1+R)}(|\sigma_1-\sigma_2|^m)\right)^{\frac{1}{m}} \le \sigma_Y \tag{11}$$

Z is formulated on taking the hydrostatic stress as numerator and the Left hand side of Eqs. (7-11) as denominator. On opening modulus sign the equations within various limits of polar angle are shown below. (for full derivation see Appendix (c))

Case I: A=B=0,F=G,H=0

$$Z=\begin{cases}\dfrac{2}{3}\left[\dfrac{(1+R)}{\left[(1+2R)\left\{\left(1+\sin\dfrac{\theta}{2}\right)^{m}+\left(1-\sin\dfrac{\theta}{2}\right)^{m}\right\}-R\,2^{m}\right]}\right]^{\frac{1}{m}} & (0\le\theta<\pi)\\ -\dfrac{2}{3}\left[\dfrac{(1+R)}{\left[(1+2R)\left\{\left(1+\sin\dfrac{\theta}{2}\right)^{m}+\left(1-\sin\dfrac{\theta}{2}\right)^{m}\right\}-R\,2^{m}\right]}\right]^{\frac{1}{m}} & (\pi\le\theta<2\pi)\end{cases} \tag{12}$$

Case II: A=B,C=0,F=G=0

$$Z=\begin{cases}\dfrac{2}{3}\left[\dfrac{\left\{1-2^{m-1}\right\}(1+R)}{\left[\left\{(2)^{m-1}(1-R)+(R+2)\right\}\left(2\sin\dfrac{\theta}{2}\right)^{m}\right.}\right.\\ \left.\left.-\left\{\left(1+3\sin\dfrac{\theta}{2}\right)^{m}+\left(1-3\sin\dfrac{\theta}{2}\right)^{m}\right\}\right]\end{cases}^{\frac{1}{m}} \quad \left(0\le\theta<2\sin^{-1}\frac{1}{3}\right)$$

* *+ve* when m is even ,-ve when m is odd

$$\begin{cases}\dfrac{2}{3}\left[\dfrac{\left\{1-2^{m-1}\right\}(1+R)}{\left[\left\{(2)^{m-1}(1-R)+(R+2)\right\}\left(2\sin\dfrac{\theta}{2}\right)^{m}\right.}\right.\\ \left.\left.-\left\{\left(1+3\sin\dfrac{\theta}{2}\right)^{m}\pm\left(1-3\sin\dfrac{\theta}{2}\right)^{m}\right\}\right]\end{cases}^{\frac{1}{m}} \quad \left(2\sin^{-1}\frac{1}{3}\le\theta<\pi\right) \tag{13a}$$

$*+ve$ when m is even,-ve when m is odd

$$Z=\begin{cases}-\frac{2}{3}\left[\dfrac{\left\{1-2^{m-1}\right\}(1+R)}{\left[\begin{array}{l}\left\{(2)^{m-1}(1-R)+(R+2)\right\}\left(2\sin\frac{\theta}{2}\right)^{m}\\ -\left\{\left(1+3\sin\frac{\theta}{2}\right)^{m}\pm\left(1-3\sin\frac{\theta}{2}\right)^{m}\right\}\end{array}\right]}\right]^{\frac{1}{m}} & \left(\pi\le\theta<2\pi-2\sin^{-1}\frac{1}{3}\right)\\ -\frac{2}{3}\left[\dfrac{\left\{1-2^{m-1}\right\}(1+R)}{\left[\begin{array}{l}\left\{(2)^{m-1}(1-R)+(R+2)\right\}\left(2\sin\frac{\theta}{2}\right)^{m}\\ -\left\{\left(1+3\sin\frac{\theta}{2}\right)^{m}+\left(1-3\sin\frac{\theta}{2}\right)^{m}\right\}\end{array}\right]}\right]^{\frac{1}{m}} & \left(2\pi-2\sin^{-1}\frac{1}{3}\le\theta<2\pi\right)\end{cases} \tag{13b}$$

Case III: A=B,C=0,F=G,H=0

$$Z=\begin{cases}\frac{2}{3}\left[\dfrac{\left\{2+2^{m-1}\right\}(1+R)}{\left[\begin{array}{l}\left\{(2)^{m-1}(1-R)+(R+2)\right\}\left\{\left(1+\sin\frac{\theta}{2}\right)^{m}+\left(1-\sin\frac{\theta}{2}\right)^{m}\right\}\\ +R\left\{\left(1+3\sin\frac{\theta}{2}\right)^{m}+\left(1-3\sin\frac{\theta}{2}\right)^{m}\right\}\end{array}\right]}\right]^{\frac{1}{m}} & \left(0\le\theta<2\sin^{-1}\frac{1}{3}\right)\\ *+ve \text{ when } m \text{ is even,-}ve \text{ when } m \text{ is odd} & \\ \frac{2}{3}\left[\dfrac{\left\{2+2^{m-1}\right\}(1+R)}{\left[\begin{array}{l}\left\{(2)^{m-1}(1-R)+(R+2)\right\}\left\{\left(1+\sin\frac{\theta}{2}\right)^{m}+\left(1-\sin\frac{\theta}{2}\right)^{m}\right\}\\ +R\left\{\left(1+3\sin\frac{\theta}{2}\right)^{m}\pm\left(1-3\sin\frac{\theta}{2}\right)^{m}\right\}\end{array}\right]}\right]^{\frac{1}{m}} & \left(2\sin^{-1}\frac{1}{3}\le\theta<\pi\right),\end{cases} \tag{14a}$$

* $+ve$ when m is even,-ve when m is odd

$$Z = \begin{cases} -\frac{2}{3}\left[\frac{\left\{2+2^{m-1}\right\}(1+R)}{\left[\left\{(2)^{m-1}(1-R)+(R+2)\right\}\left\{\left(1+\sin\frac{\theta}{2}\right)^m+\left(1-\sin\frac{\theta}{2}\right)^m\right\}\right.}\right.^{\frac{1}{m}} & \left(\pi \le \theta < 2\pi - 2\sin^{-1}\frac{1}{3}\right) \\ \left.\left.+R\left\{\left(1+3\sin\frac{\theta}{2}\right)^m \pm\left(1-3\sin\frac{\theta}{2}\right)^m\right\}\right] & \\ -\frac{2}{3}\left[\frac{\left\{2+2^{m-1}\right\}(1+R)}{\left[\left\{(2)^{m-1}(1-R)+(R+2)\right\}\left\{\left(1+\sin\frac{\theta}{2}\right)^m+\left(1-\sin\frac{\theta}{2}\right)^m\right\}\right.}\right.^{\frac{1}{m}} & \left(2\pi - 2\sin^{-1}\frac{1}{3} \le \theta < 2\pi\right) \\ \left.\left.+R\left\{\left(1+3\sin\frac{\theta}{2}\right)^m+\left(1-3\sin\frac{\theta}{2}\right)^m\right\}\right] & \end{cases} \tag{14b}$$

Case IV: A=B=0,F=G=0

$$Z = \begin{cases} \frac{2^{\frac{1}{m}}}{3}\left[\frac{(1+R)}{\left\{1+(1+2R)\left(\sin\frac{\theta}{2}\right)^m\right\}}\right]^{\frac{1}{m}} & (0 \le \theta < \pi) \\ -\frac{2^{\frac{1}{m}}}{3}\left[\frac{(1+R)}{\left\{1+(1+2R)\left(\sin\frac{\theta}{2}\right)^m\right\}}\right]^{\frac{1}{m}} & (\pi \le \theta < 2\pi) \end{cases} \tag{15}$$

Case V: A=B=C=0,F=G

$$Z = \begin{cases} \frac{2}{3}\left[\frac{(1+R)}{\left\{\left(1+\sin\frac{\theta}{2}\right)^m+\left(1-\sin\frac{\theta}{2}\right)^m+R\left(2\sin\frac{\theta}{2}\right)^m\right\}}\right]^{\frac{1}{m}} & (0 \le \theta < \pi) \\ -\frac{2}{3}\left[\frac{(1+R)}{\left\{\left(1+\sin\frac{\theta}{2}\right)^m+\left(1-\sin\frac{\theta}{2}\right)^m+R\left(2\sin\frac{\theta}{2}\right)^m\right\}}\right]^{\frac{1}{m}} & (\pi \le \theta < 2\pi) \end{cases} \tag{16}$$

Positive sign of Z for the range of θ indicates the tensile loading whereas negative sign indicates compressive loading similar to the sign convention that applies to stress triaxiality.

3.2 Plastic zone determination

In crack front, the distance from crack tip to the end point of plastic zone envelope accounts for the sustainability of stress against crack propagation or in other words the direction where the envelope is spread is safe against crack propagation. For example, if there is negligible radial distance between the crack tip and envelope then the shape of the plastic zone will reduce which implies that the crack shall require minimum amount of energy to propagate. On the other hand, as the radial distance of envelope increases the crack would require more energy to propagate.

Substituting the value of principal stresses from Eq. (3) in Eqs. (7-11), the equation of plastic zone is obtained and is expressed in terms of non-dimensional distance $\frac{r}{K_I^2/\sigma_Y^2\pi}$ (the correction factor of K_I is shown in Appendix (d)) for each of the cases as below

Case I: A=B=0,F=G,H=0

$$\frac{r_\theta}{r_y}=\frac{1}{2}\cos^2\frac{\theta}{2}\left[\begin{array}{l}\frac{1+2R}{1+R}\left\{\left(1+\sin\frac{\theta}{2}\right)^m+\left(1-\sin\frac{\theta}{2}\right)^m\right\}\\-\frac{R}{1+R}2^m\end{array}\right]^{\frac{2}{m}}\quad(0\le\theta<2\pi)\tag{17}$$

Case II: A=B,C=0,F=G=0

$$\text{For } 0\le\theta<2\sin^{-1}\frac{1}{3}\ \&\ \left(2\pi-2\sin^{-1}\frac{1}{3}\right)\le\theta<2\pi$$

$$\frac{r_\theta}{r_y}=\frac{1}{2}\cos^2\frac{\theta}{2}\left[\begin{array}{l}\frac{\left\{2^{m-1}(1-R)+(R+2)\right\}}{(1-2^{m-1})(1+R)}\left(2\sin\frac{\theta}{2}\right)^m\\-\frac{1}{(1-2^{m-1})(1+R)}\left\{\left(1+3\sin\frac{\theta}{2}\right)^m+\left(1-3\sin\frac{\theta}{2}\right)^m\right\}\end{array}\right]^{\frac{2}{m}}\tag{18a}$$

And

$$\text{For } 2\sin^{-1}\frac{1}{3}\le\theta<2\pi,\ *+\text{ ve when m is even \& -ve when m is odd}$$

$$\frac{r_\theta}{r_y}=\frac{1}{2}\cos^2\frac{\theta}{2}\left[\begin{array}{l}\frac{\left\{2^{m-1}(1-R)+(R+2)\right\}}{(1-2^{m-1})(1+R)}\left(2\sin\frac{\theta}{2}\right)^m\\-\frac{1}{(1-2^{m-1})(1+R)}\left\{\left(1+3\sin\frac{\theta}{2}\right)^m\pm\left(1-3\sin\frac{\theta}{2}\right)^m\right\}\end{array}\right]^{\frac{2}{m}}\tag{18b}$$

Case III: A=B,C=0,F=G,H=0

$$\text{For } 0\le\theta<2\sin^{-1}\frac{1}{3}\&\left(2\pi-2\sin^{-1}\frac{1}{3}\right)\le\theta<2\pi$$

$$\frac{r_\theta}{r_y}=\frac{1}{2}\cos^2\frac{\theta}{2}\left[\begin{array}{l}\frac{\left\{2^{m-1}(1-R)+R+2\right\}}{(2+2^{m-1})(1+R)}\left\{\left(1+\sin\frac{\theta}{2}\right)^m+\left(1-\sin\frac{\theta}{2}\right)^m\right\}\\+\frac{R}{(2+2^{m-1})(1+R)}\left\{\left(1+3\sin\frac{\theta}{2}\right)^m+\left(1-3\sin\frac{\theta}{2}\right)^m\right\}\end{array}\right]^{\frac{2}{m}}\tag{19a}$$

And

For $2\sin^{-1}\frac{1}{3} \le \theta < 2\pi$,*+ve when m is even & -ve when m is odd

$$\frac{r_\theta}{r_y} = \frac{1}{2}\cos^2\frac{\theta}{2}\left[\begin{array}{l}\dfrac{\left\{2^{m-1}(1-R)+R+2\right\}}{\left(2+2^{m-1}\right)(1+R)}\left\{\left(1+\sin\dfrac{\theta}{2}\right)^m+\left(1-\sin\dfrac{\theta}{2}\right)^m\right\} \\ +\dfrac{R}{\left(2+2^{m-1}\right)(1+R)}\left\{\left(1+3\sin\dfrac{\theta}{2}\right)^m \pm\left(1-3\sin\dfrac{\theta}{2}\right)^m\right\}\end{array}\right]^{\frac{2}{m}} \tag{19b}$$

Case IV:A=B=0,F=G=0

$$\frac{r_\theta}{r_y} = \frac{1}{2}\cos^2\frac{\theta}{2}\left[\frac{1+2R}{2(1+R)}\left(2\sin\frac{\theta}{2}\right)^m+\frac{1}{2(1+R)}2^m\right]^{\frac{2}{m}} \quad (0 \le \theta < 2\pi) \tag{20}$$

Case V: A=B=C=0,F=G

$$\frac{r_\theta}{r_y} = \frac{1}{2}\cos^2\frac{\theta}{2}\left[\begin{array}{l}\dfrac{1}{1+R}\left\{\left(1+\sin\dfrac{\theta}{2}\right)^m+\left(1-\sin\dfrac{\theta}{2}\right)^m\right\} \\ +\dfrac{R}{1+R}\left(2\sin\dfrac{\theta}{2}\right)^m\end{array}\right]^{\frac{2}{m}} \quad (0 \le \theta < 2\pi) \tag{21}$$

4 RESULTS AND DISCUSSION

Eqs. (7-11) are referred from [20], do show convexity for specific combination of degree of anisotropy and Lankford's coefficient as shown in Table 1. This fact provides the motivation to study the observations in the cracked plate possessing anisotropic material behavior. In order to do so, the mathematical framework of stress triaxiality has been implemented to investigate both isotropic and anisotropic materials. Fig. 1 depicts the sample of edge cracked thin sheet showing state of stress under mode-I loading condition.

Variation of *Z*, with respect to θ and plastic zone shapes, at crack tip has been plotted using numerical evaluation of Eqs. (12-21) respectively. The values of Lankford's coefficient considered are in the same domain as depicted in [21] for few practical sheet metals.

Table 1
Combination of *R* and *m* for convexity of yield loci.

Case	m	R-value)
I	can take only value as 2	correspondingly there is no restriction
II	can take only value as 2	correspondingly restricted up to value approximately value as 4
III	up to less and equal to value 2	correspondingly there is no restriction
	greater than value 2	correspondingly there is a restriction and the value go on decreasing very steeply.
IV	No boundaries of m and R-value	
V	No boundaries of m and R-value	

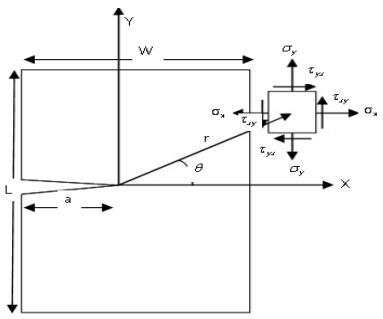

Fig.1
Model of thin sheet metal plate containing an edge crack.

4.1 Case I
4.1.1 Convexity

Fig. 2 (a) show variation of Z with θ at m=2 for various R-values. In this case convexity of yield locus, with increasing R-values, is only for m=2 [28]. The magnitude of criticality of Z increases with R-value. For this particular value of m (i.e. 2) all cases exhibit exactly similar variation. While, with increase in R-value criticality increase, the radial distance along the crack plane shrinks as shown in Fig. 2 (b). The increase of value of stress triaxiality leads to the chance for crack to propagate.

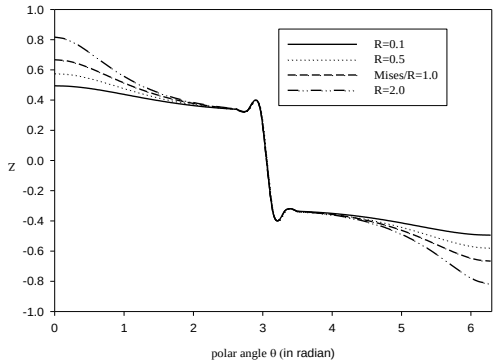

(a)
Variation of M-criteria with polar angle for m=2 in case I

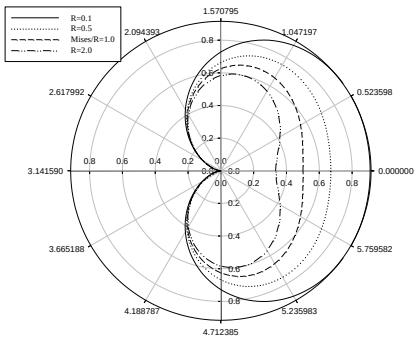

(b)
Plastic zone sizes for m=2 with varying R-values in case I

Fig.2
Variation of M-criteria with polar angle and plastic zones for convexity regions for case I,II.

4.1.2 Concavity

At R=0.5, when m>2.9 and attain even and fractional values, critical value of Z and the slope of anisotropic stress triaxiality are undefined. When m>2.9 and attain odd values, critical value of Z has been found to be at angles other than zero degree, the slope has been found to change drastically at those angles. Fig. 3(a), for example, shows that for m=5, the drastic change happens to be at 60° and 300°, for m=7 it happens to be at 80° and 280° while for m=9 at 90° and 270°. A sharp dip at these angles in polar plots of plastic zone has also been observed as shown in Fig. 3(b). At R=2, similar trends has been observed as m exceed the value 2.3. Slope changing drastically, critical Z value reaches in undefined or infinite region all signify that there is a sudden opening of yield loci which may lead to fracture.

4.2 Case II
4.2.1 Convexity

Full convexity of yield locus here happens to be for limited R-values i.e. up to 4 approximately and only for m=2 [28]. Similar trend of slope is observed as in Case I.

4.2.2 Concavity

At R=0.5, though criticality occurred at 0°, for all fractional values of m the values of Z are undefined at most of angles. As shown in Fig. 3(c) the trend of m=2 is different from that of m=3, 4, 5, 6 etc. For values of m greater than 2 i.e. 3, 4, 5 etc. there has been sharp dip observed at zero degree in polar plot of plastic zone. The shapes of plastic zone observed for values of m greater than 2 models plain strain rather than plane stress. At R=2, similar trends are observed.

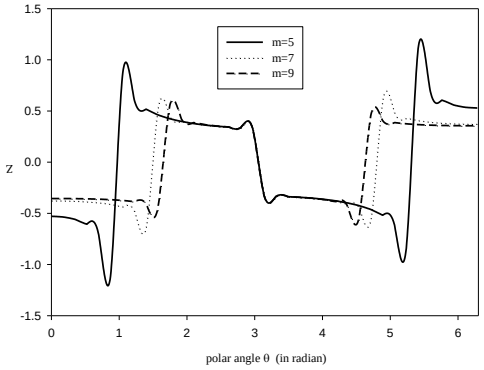

(a)
Anomalous behaviour of Z for regions other than convexity for case I

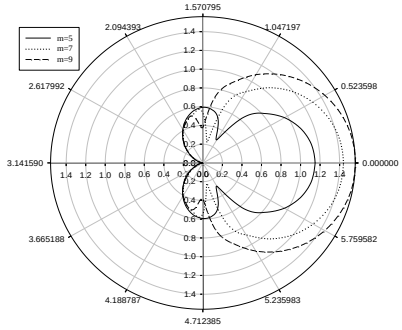

(b)
Plastic zone shapes for region other than convexity in case I

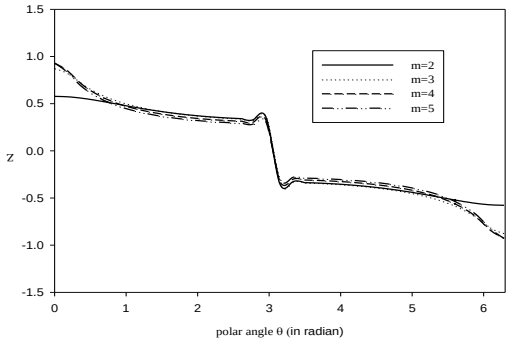

(c)
Anomalous behavior of *Z* for case II

Fig.3
Anomalous behavior of *Z* with respect to polar angle and plastic zone shapes for case I, II.

4.3 Case III
4.3.1 Convexity

In this case, *m* and *R*-value exist in such a combination that for higher order of *m* the range of *R*-value goes on decreasing for convexity of yield loci. This combination is shown in Table 1. For *m*=2, trend slope and plastic zone shapes are same as discussed for above two cases. At *m*=3 the variations are shown in Figs. 4(a) and (b). For a particular *R*-value it has been observed that as *m* increased the magnitude of *Z* also increased. It has been also shown that for the combination *R*=1, *m*=2 stress triaxiality curve coincides with *Z* curve.

4.3.2 Concavity

At *R*=0.5, though criticality occurred at 0° as in case II, for all fractional values of *m* the values of *Z* are undefined at most of angles. Though unlike case II the trend of *Z* curve for *m*=2 and higher values has been similar. At *R*=2, when m attain values even other than 2 or fractional values, critical *Z* value is undefined at certain angles. When *m*>3 and attains higher odd values i.e. 5, 7, etc. critical value of *Z* shift from 0° to other angles as shown in Fig. 4(c) and slope changes drastically at these angles.

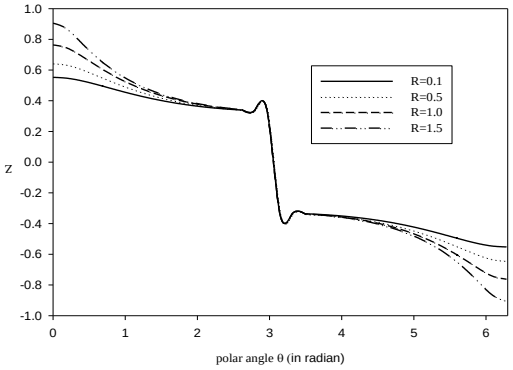

(a)
Variation of *M*-criteria with polar angle for *m*=3 in case III

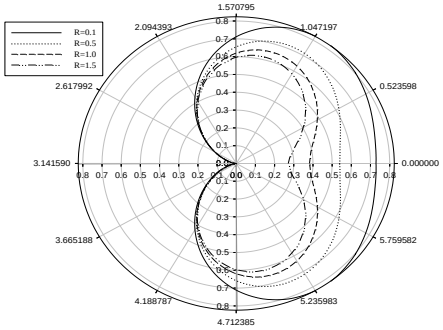

(b)
Plastic zone sizes for *m*=3 with varying *R*-values in case III

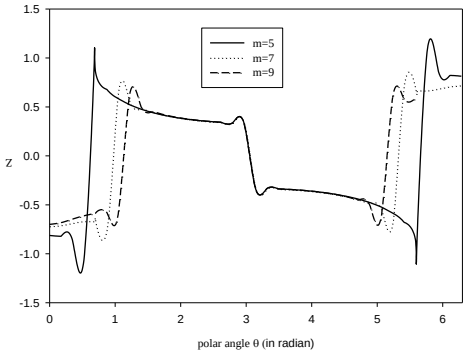

(c)
Anomalous behavior of Z for case III

Fig.4
Variation of *M*-criteria with polar angle and plastic zones for convexity regions for case III.

4.4 Case-IV

There are no such limitations of combination of *R* and *m* as far as convexity of yield locus is concerned in this case. For *m*=2, the trend of slope remains similar to above cases. For *m*=3, the *Z* variation is shown in Fig. 5(a). Plastic zone shape is shown in Fig. 5(b). Similarly, Figs. 5(c) and (d) are for *m*=4. It has been observed that as *m* increased, critical *Z* value decreased, for a particular *R*-value which is unlike and opposite to case III. Figs. 5(e) and (f) show the comparison of *Z* curve for increasing *m* and at a particular *R*-value (in this case taken as 0.5).

4.5 Case V

Similar to case IV, in case V too, there is no limitation of combination to convexity of yield locus. Again for *m*=2 the result is similar to above four cases. The critical value of *Z* increases with increase in *R*-value, but decreased with increasing *m.* On comparing case IV and V for a particular value of *m* and *R,* higher magnitude of critical *Z* is observed in case V. Figs. 6(a) and (b) show trend for *m*=3 for increasing *R*, whereas Figs. 6(c) and (d) show for *m*=4. Figs. 6(e) and (f) show comparison of *Z* with increasing *m* at a particular *R*-value (in this case the value taken is 2).

For the first three cases at combinations of *R* and *m* other than that has been defined for convexity, i.e. for concave and unbounded region the anomalous behavior of *Z* has been observed Figs. 3(a) and (b) show this behavior for case I, Fig. 3(c) shows for case II and Fig. 4(c) for case III. The behavior observed is such that for these

combinations the polar angle at which criticality of *Z* is observed shifts from 0 degree and *Z* value is undefined for certain angles or the slope of *Z* drastically changes at these angles.

Plastic zone shapes and *Z*-curves are found to complement each other, as at angles where the triaxiality reaches its critical value the radius of plastic zone shrinks to minimum at those angles.

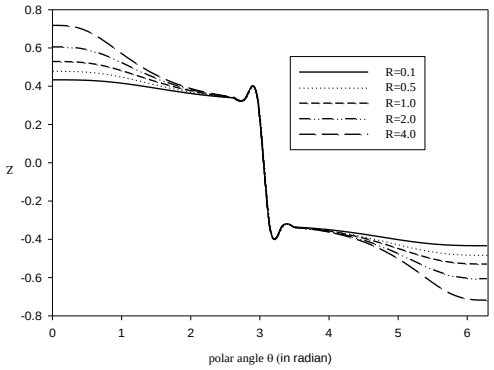

(a)
Variation of *M*-criteria with polar angle for *m*=3 in case IV

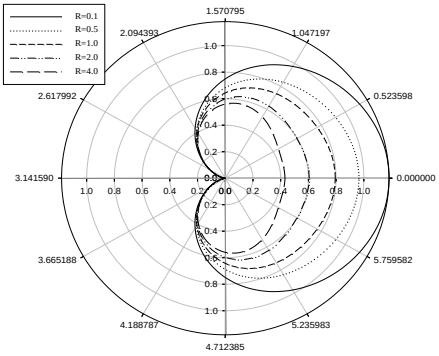

(b)
Plastic zone sizes for *m*=3 with varying *R*-values in case IV

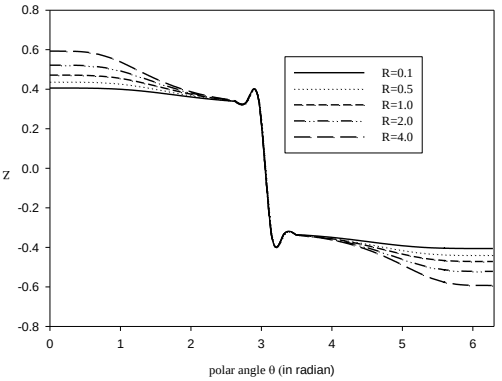

(c)
Variation of *M*-criteria with polar angle for *m*=4 in case IV

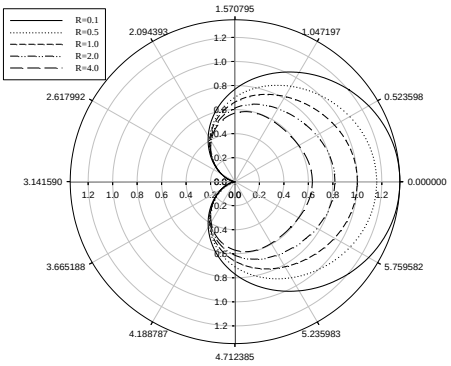

(d)
Plastic zone sizes for *m*=4 with varying *R*-values in case IV

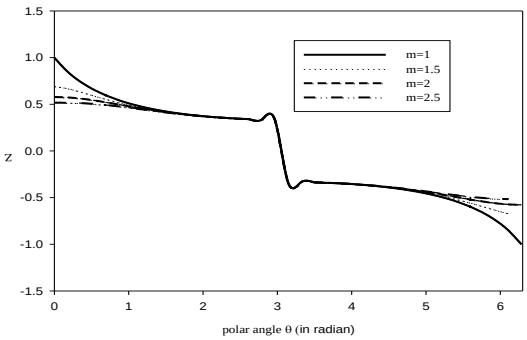

(e)
Variation of *M*-criteria with polar angle for increasing m at *R*=0.5 in case IV

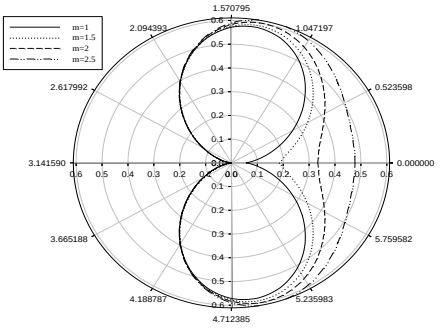

(f)
Plastic zone sizes for increasing *m* at *R*=0.5 in case IV

Fig.5
Variation of *M*-criteria with polar angle and plastic zones for convexity regions for case IV.

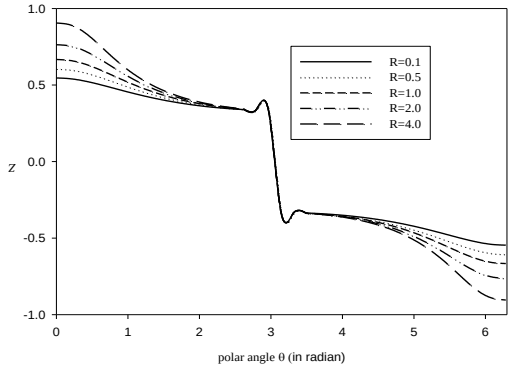

(a)

Variation of *M*-criteria with polar angle for *m*=3 in case V

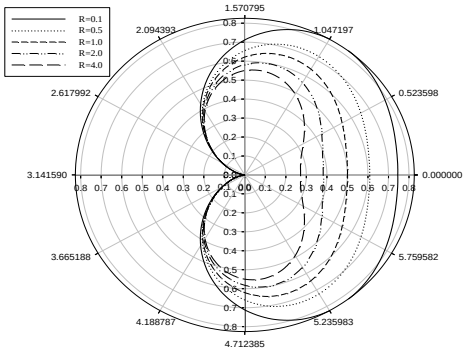

(b)

Plastic zone sizes for *m*=3 with varying *R*-values in case V

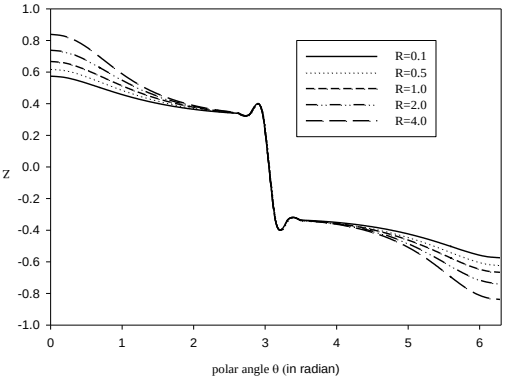

(c)

Variation of *M*-criteria with polar angle for *m*=4 in case V

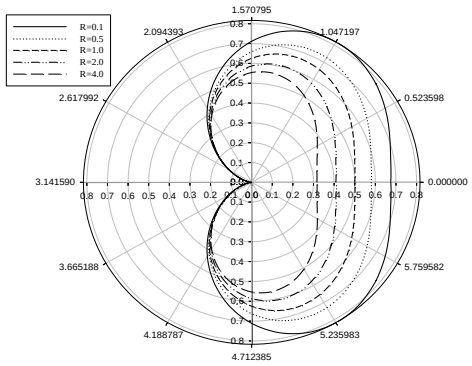

(d)

Plastic zone sizes for *m*=4 with varying *R*-values in case V

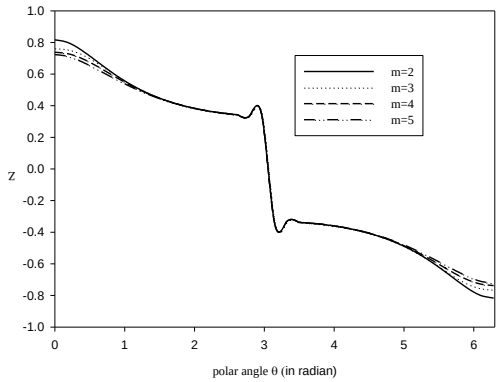

(e)

Variation of *M*-criteria with polar angle for increasing *m* at *R*=2 in case V

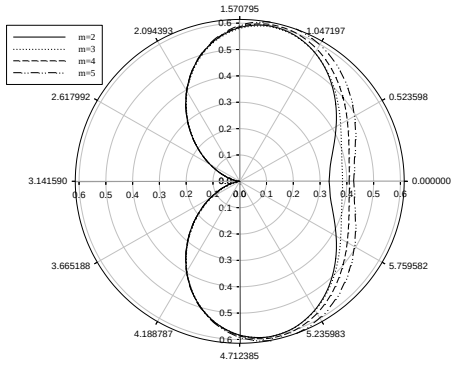

(f)

Plastic zone sizes for increasing *m* at *R*=2 in case V

Fig.6

Variation of *M*-criteria with polar angle and plastic zones for convexity regions for case V.

5 CONCLUSIONS

A thin sheet metal plate exhibiting anisotropic plane stress condition, containing edge crack under mode-I loading condition has been considered as a problem under investigation. Five cases of plane stress condition were taken into consideration. A crack tip constraint has been formulated, in the form of ratio of hydrostatic to Hill's equivalent stress to predict onset of crack propagation. Formulation of this constraint also involves important anisotropic parameters, which reveal material behavior. Stress triaxiality, one of the most important ductile fracture parameter was found to be the part of this generalized formulation, and coincided with generalized curve for m=2 and R=1. Investigation revealed that the critical values of this formulated constraint are almost in the same domain when compared to the values of stress triaxiality [22]. Investigation also showed unbounded regions and of concavity of yield loci since in those regions either the slope showed drastic change, or the curve of the constraint showed anomalous behavior i.e. critical value was found to be undefined or infinite.

As far as convexity of yield loci is considered, following conclusions have been withdrawn upon critical examination of various equations of Z developed for all the five cases:

i All the cases are same for quadratic degree of anisotropy since the critical values obtained in each of them were equal.

ii In each of the cases increase of Lankford's coefficient leads to increase the criticality of constraint.

iii When Lankford's coefficient attained value less than unity, case III and V showed similar trend of constraint curve i.e. with increase in degree of anisotropy the critical value increased but in case IV, it showed contrary behavior to above i.e. criticality decreased with increase in degree of anisotropy.

iv When Lankford's coefficient attained value greater than unity case IV and V showed similar trend of constraint curve i.e. with increase in degree of anisotropy, the critical value decreased but in case III, criticality increased with increase in degree of anisotropy.

v The percent increase or decrease in critical value of a crack tip constraint were found to be different when cases III, IV and V were compared on basis of variation in Lankford's coefficient and degree of anisotropy.

vi While designing the components designers should take stress triaxiality under consideration because its critical value is important. The principal stresses corresponding to the critical value of constraint Z can be considered as one of the design criterion which plays a vital role in automobile and aerospace industries.

APPENDIX A

Stress triaxiality (M) can be expressed as:

$$M = \frac{\sigma_h}{\sigma_{eqv}}$$

where σ_h is the hydrostatic stress for mode I fracture and σ_{eqv} is the Von Mises equivalent stress; hydrostatic stress in terms of principal stresses is expressed as:

$$\sigma_{\mathrm{h}} = \frac{\sigma_1 + \sigma_2 + \sigma_3}{3}$$

where $\sigma_1, \sigma_2, \sigma_3$ are the principal stress at crack tip (as given by Westergaard) and these principal stresses can be expressed in terms of stress intensity factor, radial distance from the crack tip and polar angle as:

$$\sigma_{1,2} = \frac{K_I}{\sqrt{2\pi r}} \cos\frac{\theta}{2}\left(1 \pm \sin\frac{\theta}{2}\right) \quad : \sigma_3 = 0 \left(\text{for plane stress condition}\right)$$

On substituting these principal stresses in the expression of hydrostatic stress we obtain

$$\sigma_h = \frac{\frac{K_I}{\sqrt{2\pi r}}\cos\frac{\theta}{2}\left(1+\sin\frac{\theta}{2}\right)+\frac{K_I}{\sqrt{2\pi r}}\cos\frac{\theta}{2}\left(1-\sin\frac{\theta}{2}\right)+0}{3} \qquad \sigma_h = \frac{2K_I}{3\sqrt{2\pi r}}\cos\frac{\theta}{2}$$

Von Mises equivalent stresses have the form as:

$$\sigma_{eqv} = \sqrt{\frac{1}{2}\left\{\left(\sigma_1-\sigma_2\right)^2+\left(\sigma_2-\sigma_3\right)^2+\left(\sigma_3-\sigma_1\right)^2\right\}}$$

For plane stress condition third principal stress is zero (i.e. $\sigma_3 = 0$) therefore the above expression reduces to

$$\sigma_{eqv} = \sqrt{\sigma_1^2+\sigma_2^2-\sigma_1\sigma_2}$$

On substituting the value of principal stresses in the above expression we obtain σ_{eqv} as:

$$\sigma_{eqv} = \frac{K_I}{\sqrt{2\pi r}}\left\{\cos^2\frac{\theta}{2}\left(1+\sin\frac{\theta}{2}\right)^2+\cos^2\frac{\theta}{2}\left(1-\sin\frac{\theta}{2}\right)^2-\cos^2\frac{\theta}{2}\left(1-\sin^2\frac{\theta}{2}\right)^2\right\}^{1/2}$$

On solving and cancelling the unlike terms we obtain the expression as:

$$\sigma_{eqv} = \frac{K_I}{\sqrt{2\pi r}}\left\{\left(\cos^2\frac{\theta}{2}\right)\left(1+3\sin^2\frac{\theta}{2}\right)\right\}^{1/2}$$

On substituting the simplified expressions of equivalent stress and hydrostatic stress in expression of *M* we obtain

$$M = \frac{\frac{2K_I}{3\sqrt{2\pi r}}\cos\frac{\theta}{2}}{\frac{K_I}{\sqrt{2\pi r}}\left\{\cos^2\frac{\theta}{2}\left(1+3\sin^2\frac{\theta}{2}\right)\right\}^{1/2}}$$

On cancelling the stress intensity factor term the final expression of stress triaxiality reduces to

$$M = \frac{2\cos\frac{\theta}{2}}{3\left\{\cos^2\frac{\theta}{2}\left(1+3\sin^2\frac{\theta}{2}\right)\right\}^{1/2}}$$

Cosine term is not cancelled because the denominator is always going to +ve anyways but numerator is +ve when $0 \le \theta < \pi$ and is –ve when $\pi \le \theta < 2\pi$ therefore to capture the real nature of stress triaxiality the above expression is kept as it is.

APPENDIX B

Expressions for six anisotropic constants F, G, H, L, M, N.

The six anisotropic constants can be expressed in terms of three directional normal and shear yield stresses. Equating one or more constants to zero imply that the yield stress in a particular direction is expressed in terms of the other two or vice versa. If the axes of material anisotropy are assumed to be orthogonal, we can write

$$(G+H)\left(\sigma_1^Y\right)^2=1;\qquad (F+H)\left(\sigma_2^Y\right)^2=1;\qquad (F+G)\left(\sigma_3^Y\right)^2=1$$

where $\sigma_1^Y,\sigma_2^Y,\sigma_3^Y$ is the normal yield stresses with respect to the axes of anisotropy. Therefore we have

$$F=\frac{1}{2}\left[\frac{1}{\left(\sigma_2^Y\right)^2}+\frac{1}{\left(\sigma_3^Y\right)^2}-\frac{1}{\left(\sigma_1^Y\right)^2}\right];\ G=\frac{1}{2}\left[\frac{1}{\left(\sigma_3^Y\right)^2}+\frac{1}{\left(\sigma_1^Y\right)^2}-\frac{1}{\left(\sigma_2^Y\right)^2}\right];\ H=\frac{1}{2}\left[\frac{1}{\left(\sigma_1^Y\right)^2}+\frac{1}{\left(\sigma_2^Y\right)^2}-\frac{1}{\left(\sigma_3^Y\right)^2}\right]$$

Similarly, if $\tau_{12}^Y,\tau_{23}^Y,\tau_{31}^Y$ are the yield stresses in shear (with respect to the axes of anisotropy), we have

$$L=\frac{1}{2\left(\tau_{23}^Y\right)^2};\qquad \mathrm{M}=\frac{1}{2\left(\tau_{31}^Y\right)^2};\qquad \mathrm{N}=\frac{1}{2\left(\tau_{12}^Y\right)^2}$$

APPENDIX C

Stress triaxiality for anisotropy (*Z*) /crack tip constraint can be expressed as:

$$Z=\frac{\sigma_h}{\sigma_y}$$

where σ_h is the hydrostatic stress for mode I fracture and σ_y is the yield stress (case I); hydrostatic stress in terms of principal stresses is expressed as:

$$\sigma_{\mathrm{h}}=\frac{\sigma_1+\sigma_2+\sigma_3}{3}$$

where $\sigma_1,\sigma_2,\sigma_3$ are the principal stress at crack tip (as given by Westergaard) and these principal stresses can be expressed in terms of stress intensity factor, radial distance from the crack tip and polar angle as:

$$\sigma_{1,2}=\frac{K_I}{\sqrt{2\pi r}}\cos\frac{\theta}{2}\left(1\pm\sin\frac{\theta}{2}\right)\quad :\sigma_3=0\left(\text{for plane stress condition}\right)$$

On substituting these principal stresses in the expression of hydrostatic stress we obtain

$$\sigma_h=\frac{\frac{K_I}{\sqrt{2\pi r}}\cos\frac{\theta}{2}\left(1+\sin\frac{\theta}{2}\right)+\frac{K_I}{\sqrt{2\pi r}}\cos\frac{\theta}{2}\left(1-\sin\frac{\theta}{2}\right)+0}{3}\qquad \sigma_h=\frac{2K_I}{3\sqrt{2\pi r}}\cos\frac{\theta}{2}$$

Yield stress for case I have the form as:

$$\sigma_y=\left(\frac{1+2R}{1+R}(|\sigma_1|^m+|\sigma_2|^m)-\frac{R}{1+R}|\sigma_1+\sigma_2|^m\right)^{\frac{1}{m}}$$

On substituting the principal stresses in the above expression we obtain

$$\sigma_Y = \frac{K_I}{\sqrt{2\pi r}}\left[\frac{1+2R}{1+R}\left|\cos\frac{\theta}{2}\left(1+\sin\frac{\theta}{2}\right)\right|^m + \left|\cos\frac{\theta}{2}\left(1-\sin\frac{\theta}{2}\right)\right|^m - \frac{R}{1+R}\left|\cos\frac{\theta}{2}\left(1+\sin\frac{\theta}{2}+1-\sin\frac{\theta}{2}\right)\right|^m\right]^{\frac{1}{m}}$$

On solving and cancelling the unlike terms we obtain the expression as:

$$\sigma_Y = \frac{K_I}{\sqrt{2\pi r}\,(1+R)^{1/m}}\left[(1+2R)\left\{\left|\cos\frac{\theta}{2}\left(1+\sin\frac{\theta}{2}\right)\right|^m + \left|\cos\frac{\theta}{2}\left(1-\sin\frac{\theta}{2}\right)\right|^m\right\} - R\left|2\cos\frac{\theta}{2}\right|^m\right]^{\frac{1}{m}}$$

On substituting the simplified expression of yield stress (case I) and hydrostatic stress in the expression of Z we obtain

$$Z = \frac{\frac{2K_I}{3\sqrt{2\pi r}}\cos\frac{\theta}{2}}{\frac{K_I}{\sqrt{2\pi r}\,(1+R)^{1/m}}\left[(1+2R)\left\{\left|\cos\frac{\theta}{2}\left(1+\sin\frac{\theta}{2}\right)\right|^m + \left|\cos\frac{\theta}{2}\left(1-\sin\frac{\theta}{2}\right)\right|^m\right\} - R\left|2\cos\frac{\theta}{2}\right|^m\right]^{\frac{1}{m}}}$$

On cancelling the stress intensity factor term the final expression of stress triaxiality reduces to

$$Z = \frac{2\cos\frac{\theta}{2}}{3}\left[\frac{(1+R)}{(1+2R)\left\{\left|\cos\frac{\theta}{2}\left(1+\sin\frac{\theta}{2}\right)\right|^m + \left|\cos\frac{\theta}{2}\left(1-\sin\frac{\theta}{2}\right)\right|^m\right\} - R\left|2\cos\frac{\theta}{2}\right|^m}\right]^{\frac{1}{m}}$$

For m even or odd the denominator is always +ve whereas the numerator is +ve when $0 \le \theta < \pi$ but is –ve when $\pi \le \theta < 2\pi$ therefore on opening the modulus sign and cancelling the cosine term the final expression reduces in the form

$$Z = \begin{cases} \frac{2}{3}\left[\frac{(1+R)}{\left[(1+2R)\left\{\left(1+\sin\frac{\theta}{2}\right)^m + \left(1-\sin\frac{\theta}{2}\right)^m\right\} - R\,2^m\right]}\right]^{\frac{1}{m}} & (0 \le \theta < \pi) \\ -\frac{2}{3}\left[\frac{(1+R)}{\left[(1+2R)\left\{\left(1+\sin\frac{\theta}{2}\right)^m + \left(1-\sin\frac{\theta}{2}\right)^m\right\} - R\,2^m\right]}\right]^{\frac{1}{m}} & (\pi \le \theta < 2\pi) \end{cases}$$

APPENDIX D

Stress intensity factor with edge effect and other correction factors. There are closed form solutions available for calculating the SIF for single edge crack panel, but for pure opening mode I SIF. The general form can be represented as:

$$K_I = Y\,\sigma\sqrt{a}$$

where Y is the geometric correction and it is usually a function of both crack length a and panel width w. The available geometric factor is only valid for a straight single edge crack panel is calculated as:

$$Y = 1.99 - 0.41\left(\frac{a}{w}\right) + 18.7\left(\frac{a}{w}\right)^2 - 38.48\left(\frac{a}{w}\right)^3 + 53.85\left(\frac{a}{w}\right)^4$$

REFERENCES

[1] Lou Y., Yoon J. W., Huh H., 2014, Modeling of shear ductile fracture considering a changeable cut-off value for stress triaxiality, *International Journal of Plasticity* **54**: 56-80.

[2] Ognedal A.S., Clausen A. H., Dahlen A., Hopperstad O. S., 2014, Behavior of PVC and HDPE under highly triaxial stress states: An experimental and numerical study, *Mechanics of Materials* **72**: 94-108.

[3] Lou Y., 2013, Evaluation of ductile fracture criteria in a general three-dimensional stress state considering the stress triaxiality and the, *Acta Mechanica Solida Sinica* **26**(6): 642-658.

[4] Paul S. K., 2013, Effect of martensite volume fraction on stress triaxiality and deformation behavior of dual phase steel, *Materials & Design* **50**: 782-789.

[5] Jackiewicz J., 2011, Use of a modified Gurson model approach for the simulation of ductile fracture by growth and coalescence of microvoids under low, medium and high stress triaxiality loadings, *Engineering Fracture Mechanics* **78**(3): 487-502.

[6] Peirs J., Verleysen P., Degrieck J., 2011, Experimental study of the influence of strain rate on fracture of Ti6Al4V, *Procedia Engineering* **10**: 2336-2341.

[7] Ha S., Ã K. K., 2010, Void growth and coalescence in f . c . c . single crystals, *International Journal of Mechanical Sciences* **52**(7):863-873.

[8] Trattnig G., Antretter T., Pippan R., 2008, Fracture of austenitic steel subject to a wide range of stress triaxiality ratios and crack deformation modes, *Engineering Fracture Mechanics* **75**: 223-235.

[9] Bru M., Chyra O., Albrecht D., 2008, A ductile damage criterion at various stress triaxialities, *International Journal of Plasticity* **24**:1731-1755.

[10] Zhang W., Deng X., 2007, Mixed-mode I/II fields around a crack with a cohesive zone ahead of the crack tip, *Mechanics Research Communications* **34**: 172-180.

[11] Zhu H., Zhu L., Lv X., 2007, Investigation of fracture mechanism of 6063 aluminum alloy under different stress states , *International Journal of Fracture* **146**:159-172.

[12] Bao Y., 2005, Dependence of ductile crack formation in tensile tests on stress triaxiality, stress and strain ratios, *Engineering Fracture Mechanics* **72**(4):505-522.

[13] Bao Y., Wierzbicki T., 2005, On the cut-off value of negative triaxiality for fracture, *Engineering Fracture Mechanics* **72** :1049-1069.

[14] Bao Y., Wierzbicki T., 2004, On fracture locus in the equivalent strain and stress triaxiality space, *International Journal of Mechanical Sciences* **46**: 81-98.

[15] Kim Y., Schwalbe K., 2004, Numerical analyses of strength mis-match effect on local stresses for ideally plastic materials, *Engineering Fracture Mechanics* **71**:1177-1199.

[16] Hopperstad O. S., Børvik T., Langseth M., Labibes K., Albertini C., 2003, On the influence of stress triaxiality and strain rate on the behaviour of a structural steel, *European Journal of Mechanics- A/Solids* **22**: 1-13.

[17] Shama A., Zarghamee M., Ojdrovic R., Schafer B., 2003, Seismic damage evaluation of a steel building using stress triaxiality, *Engineering Structures* **25**: 271-279.

[18] Ores B., Co M., Str A., 2001, The effect of stress triaxiality on tensile behavior of cavitating specimens, *Journal of Materials Science* **6**: 5155-5159.

[19] City K., 2000, Fracture and yield behavior of adhesively bonded joints under triaxial stress conditions, *Journal of Materials Science* **5**: 2481-2491.

[20] Zhu Y., Dodd B., Caddell R. M., Hosford W. F., 1987, Convexity restrictions on non-quadratic anisotropic yield criteria, *International Journal of Mechanical Sciences* **29**(10): 733-741.

[21] Hance B.M., 2005, Influence of Discontinuous Yielding on Normal Anisotropy (<I>R</I>-Value) Measurements, *Journal of Materials Engineering and Performance* **14**: 616-622.

[22] Bhadauria S. S., Hora M. S., Pathak K. K., 2009, Effect of stress triaxiality on yielding of anisotropic, *Journal of Solid Mechanics* **1**(3): 226-232.